Supplementary Material

Heterostructure engineering of rod-like Bi_2S_3/Bi_2Se_3 composites for high-sensitivity direct X-ray detection with ultra-low detection limit

Bolong Li,[a] Qian Ma,*[a] Pan Gao,[b] Huayushuo Zhang,[a] Xiaoxia Yang,[a] Mingming Song,[a] Chao Li,[a] Xiaomei Jiang*[b]

Preparation of pure Bi_2Se_3. Pure Bi_2Se_3 samples were also rapidly synthesized through a hydrothermal method. $Bi(NO_3)_3{\cdot}_5H_2O$ and selenium powder were mixed in a molar ratio of 1:1 and added into 20 mL of DMF, followed by stirring for 40 minutes. Subsequently, 0.0025 g of ascorbic acid and 0.01 g of CTAB were added to the mixture. The resulting mixture This solution was then transferred to a Teflon-lined autoclave was heated and maintained at 200 °C for 3.5 h. After cooling to room temperature, the black precipitate was collected by centrifugation, washed three times with ethanol and deionized water, and finally dried overnight in an oven at 60 °C to obtain black Bi_2Se_3 powders.

Details of EIS Testing. A three-electrode system was employed, where the working electrode (WE) was a fluorine-doped tin oxide (FTO) conductive glass loaded with the sample, the reference electrode (RE) was a saturated calomel electrode, and the counter electrode (CE) was a platinum (Pt) electrode. The electrolyte used was a 0.5 mol/L aqueous solution of Sodium sulfate (Na_2SO_4) prepared with ultrapure water. Na_2SO_4 was used as a neutral inert electrolyte, which can avoid chemical corrosion of the

Bi_2S_3/Bi_2Se_3 heterostructure. Additionally, the Na^+ and SO_4^{2-} ions exhibit stable mobility, which helps reduce interference from ion diffusion on the impedance signal. A DC bias potential of -1.08 V vs Ref. was applied during the test. The amplitude of the AC perturbation signal was set to 10 mV, which complies with the small-signal perturbation principle and prevents irreversible changes to the electrode surface state. The frequency scanning range was from 2×10^4 Hz (initial frequency) to 0.1 Hz (final frequency), with 10 data acquisition points per decade

Details of Powder Compaction. For the pellet-based lateral detector in this study, silver electrodes were fabricated on the pellet surface, and the electrode spacing corresponding to an active area of 0.0005 cm^2. We have precisely controlled the absorber dosage via a standardized process. Specifically, 20 mg of the powdered sample was first weighed, and the ground sample powder was then pressed into thin pellets using a manual tablet press under a pressure of 10 MPa with a holding time of 5 min. Thickness measurements of the pressed pellets showed that all pellets had a consistent thickness of 500 μm across, ensuring thickness uniformity both within and between batches[59].

Computational Details. All calculations were performed within the framework of density functional theory (DFT) as implemented in the Vienna Ab initio Simulation Package (VASP 6.3.2). The exchange-correlation functional was treated using the Perdew-Burke-Ernzerhof (PBE)

generalized gradient approximation (GGA). We employed a plane-wave basis set with a kinetic energy cutoff of 400 eV and the projector augmented wave (PAW) pseudopotentials. Brillouin zone integration was performed using a 2 × 4 × 1 Γ-centered k-point mesh. A vacuum layer exceeding 15 Å was added perpendicular to the material surface to eliminate spurious interactions between periodic images. All atomic positions and lattice constants were fully relaxed until the forces on each atom were less than 0.01 eV/Å, with an energy convergence criterion of 10^{-4} eV. For the density of states (DOS) calculations, we applied a Gaussian smearing of 0.05 eV to ensure smooth distributions.

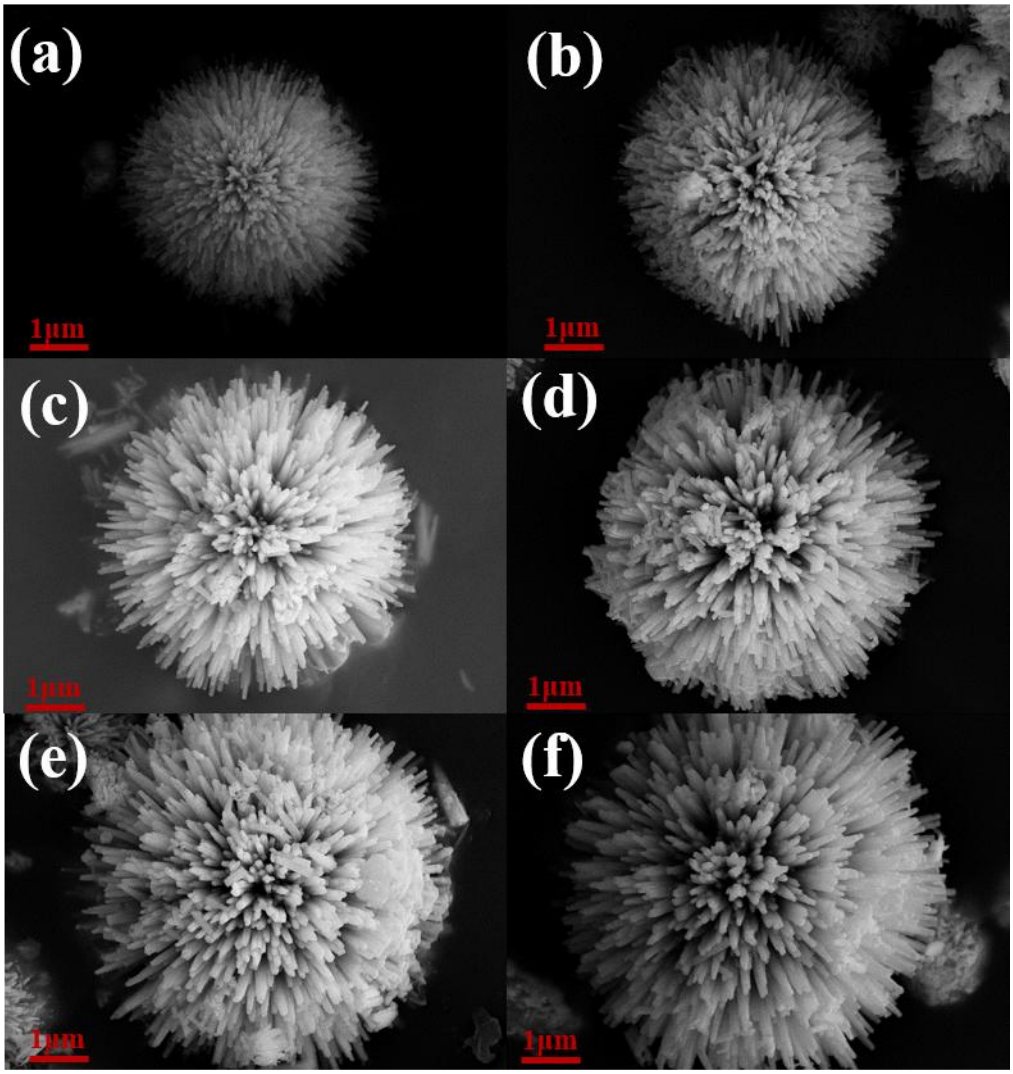

Fig. S1 SEM images of samples with different Se addition amounts.

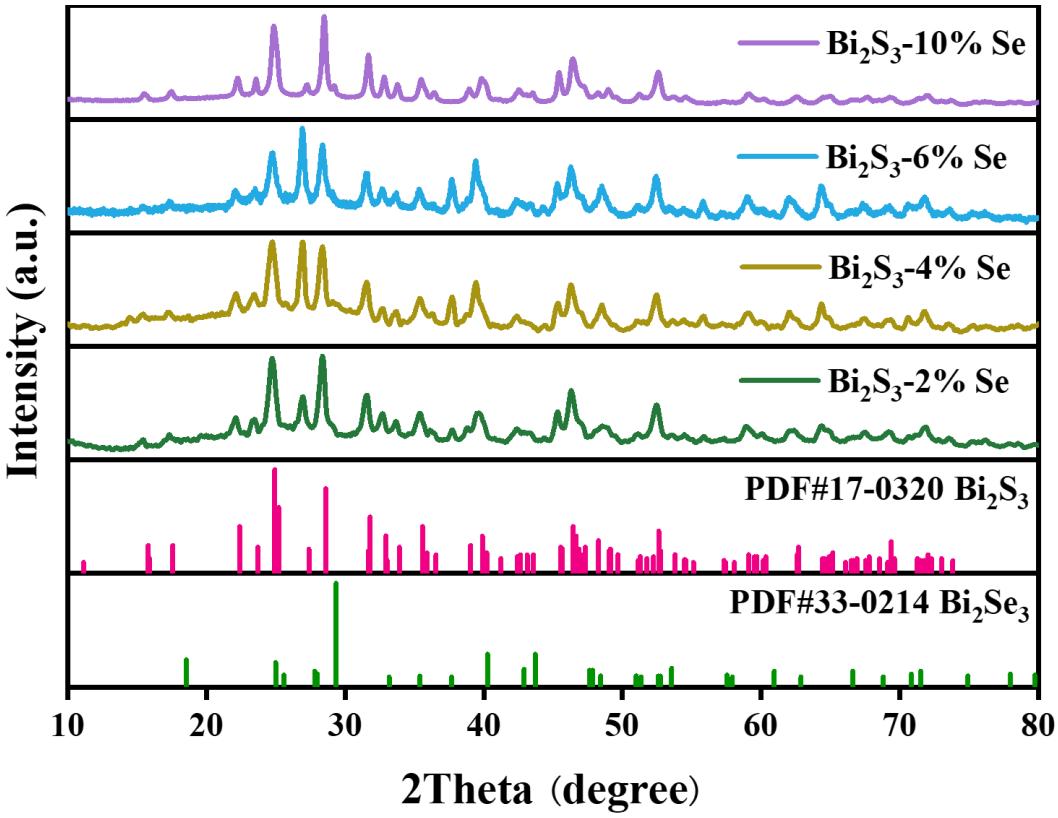

Fig. S2 XRD patterns of various samples.

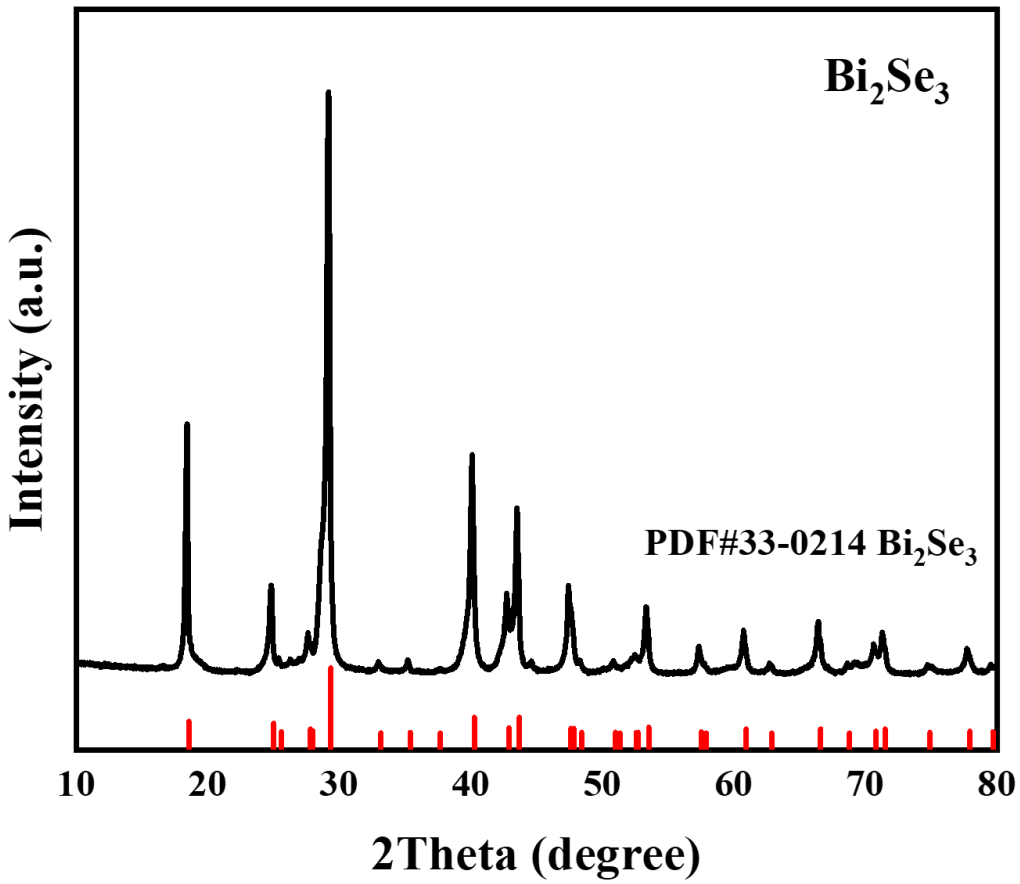

Fig. S3. XRD patterns of Bi_2Se_3.

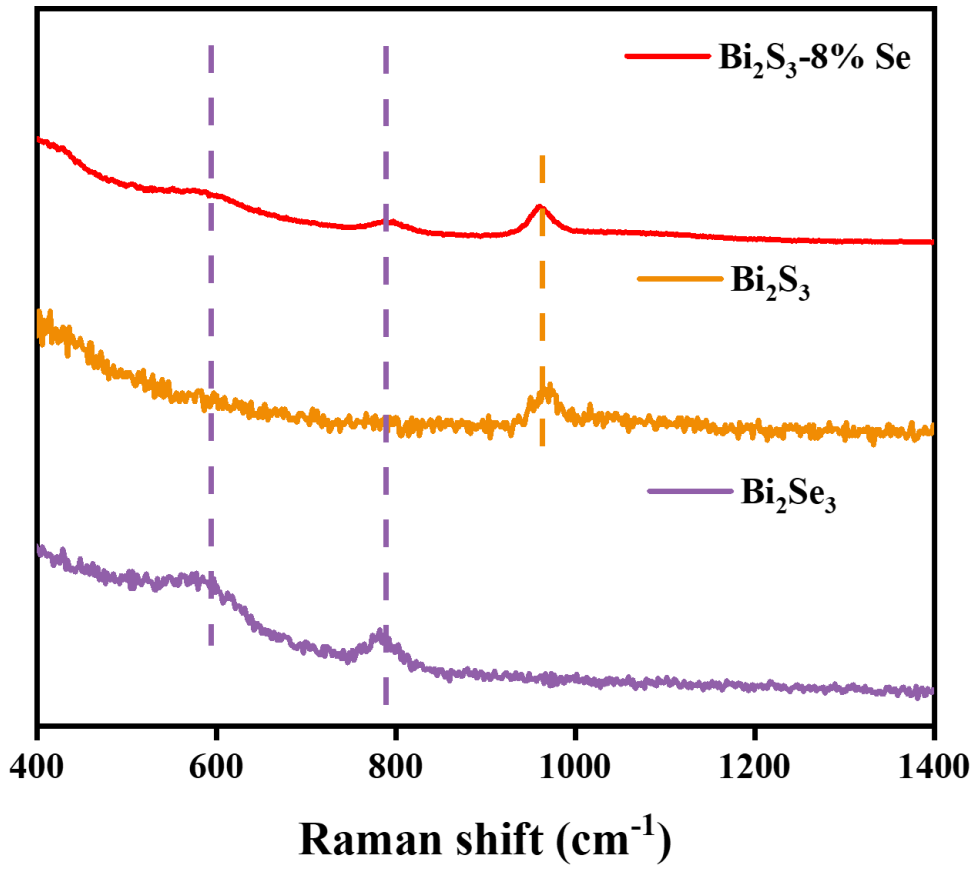

Fig. S4 The Raman spectrum of Bi_2S_3-8% Se, Bi_2S_3 and Bi_2Se_3.

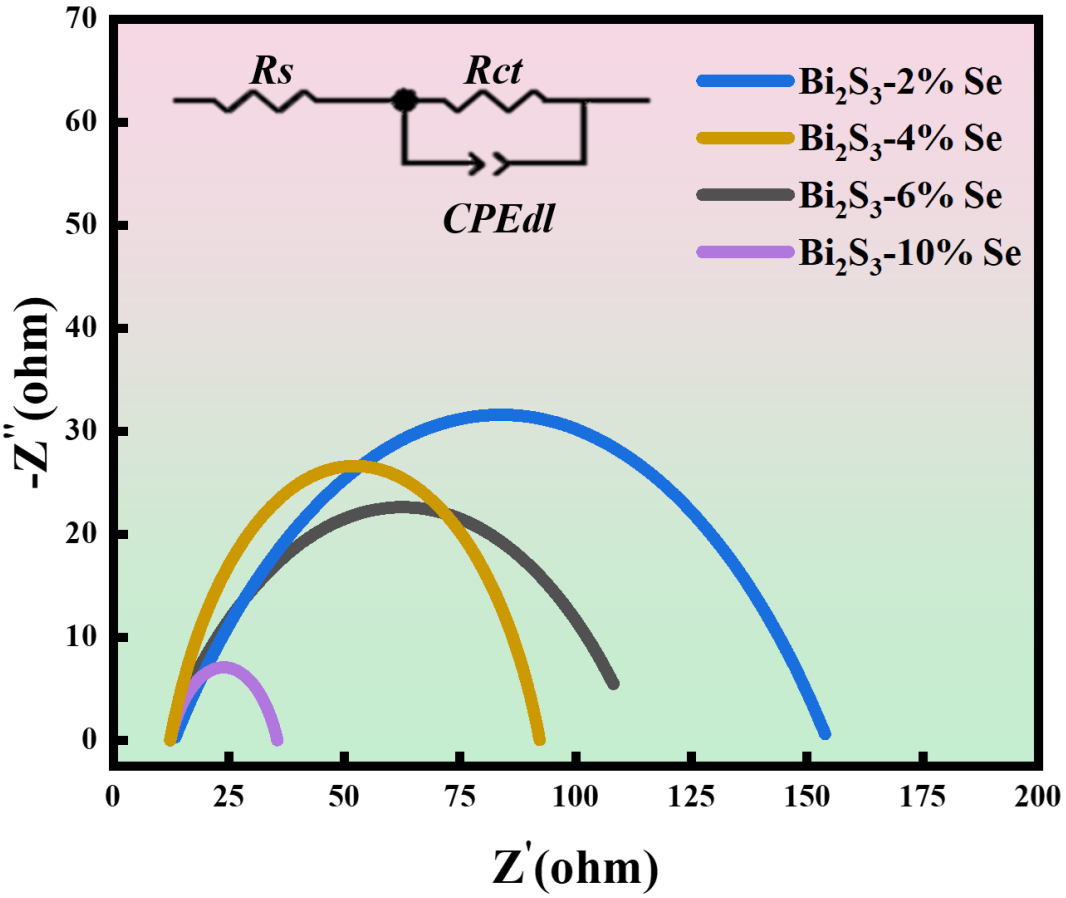

Fig. S5 Nyquist plots of different samples.

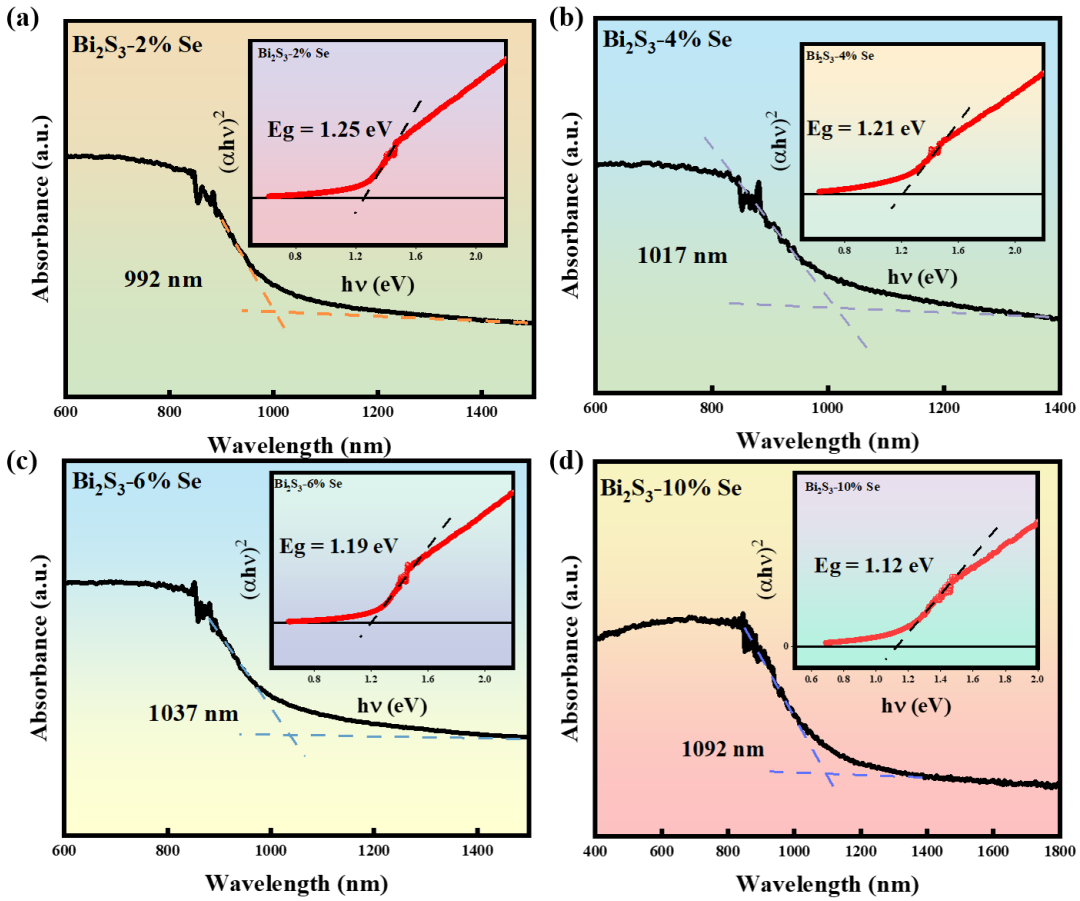

Fig. S6 UV-vis DRS of different samples.

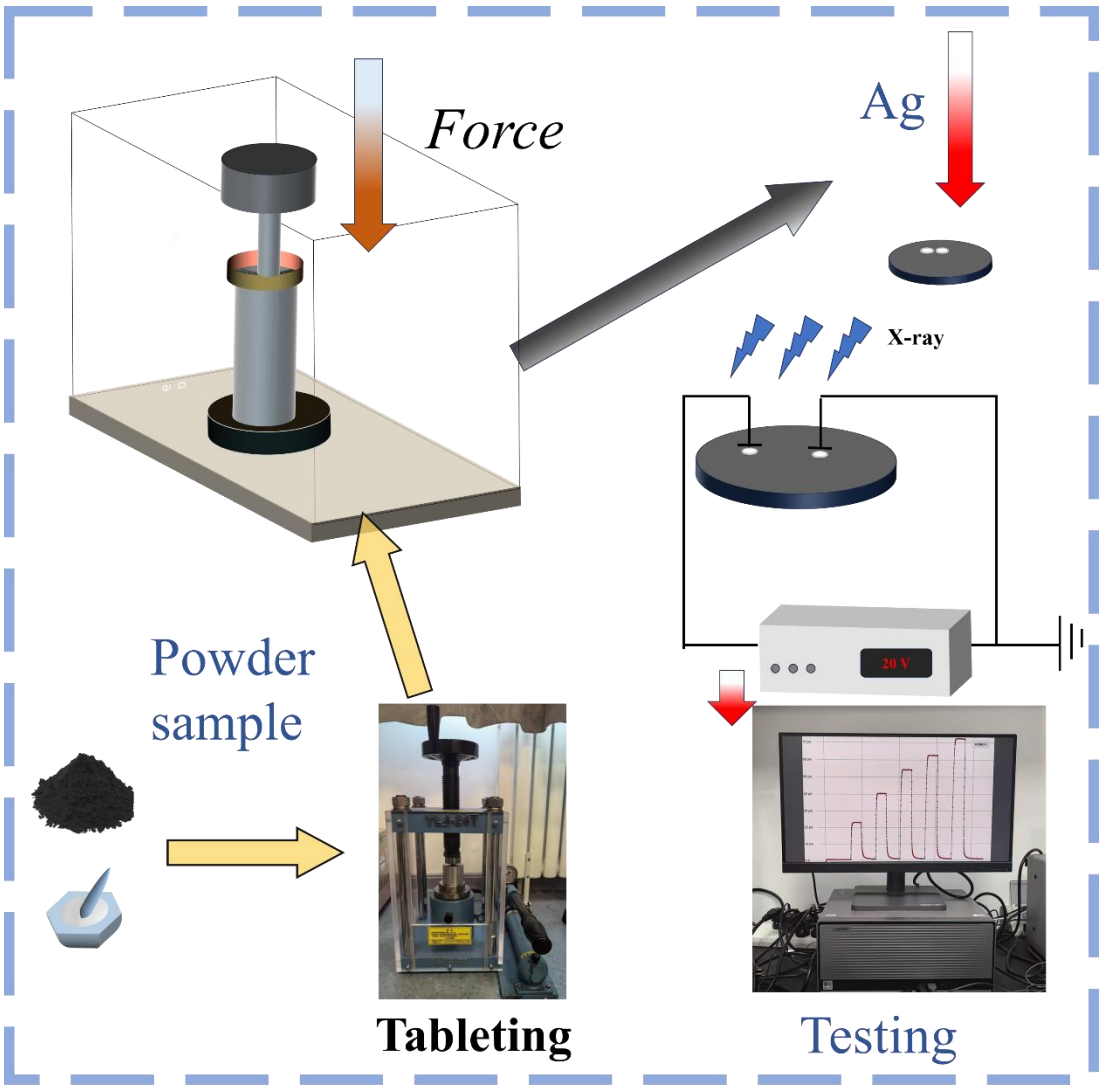

Fig. S7 Pressed pellet samples for constructing horizontal structure detectors.

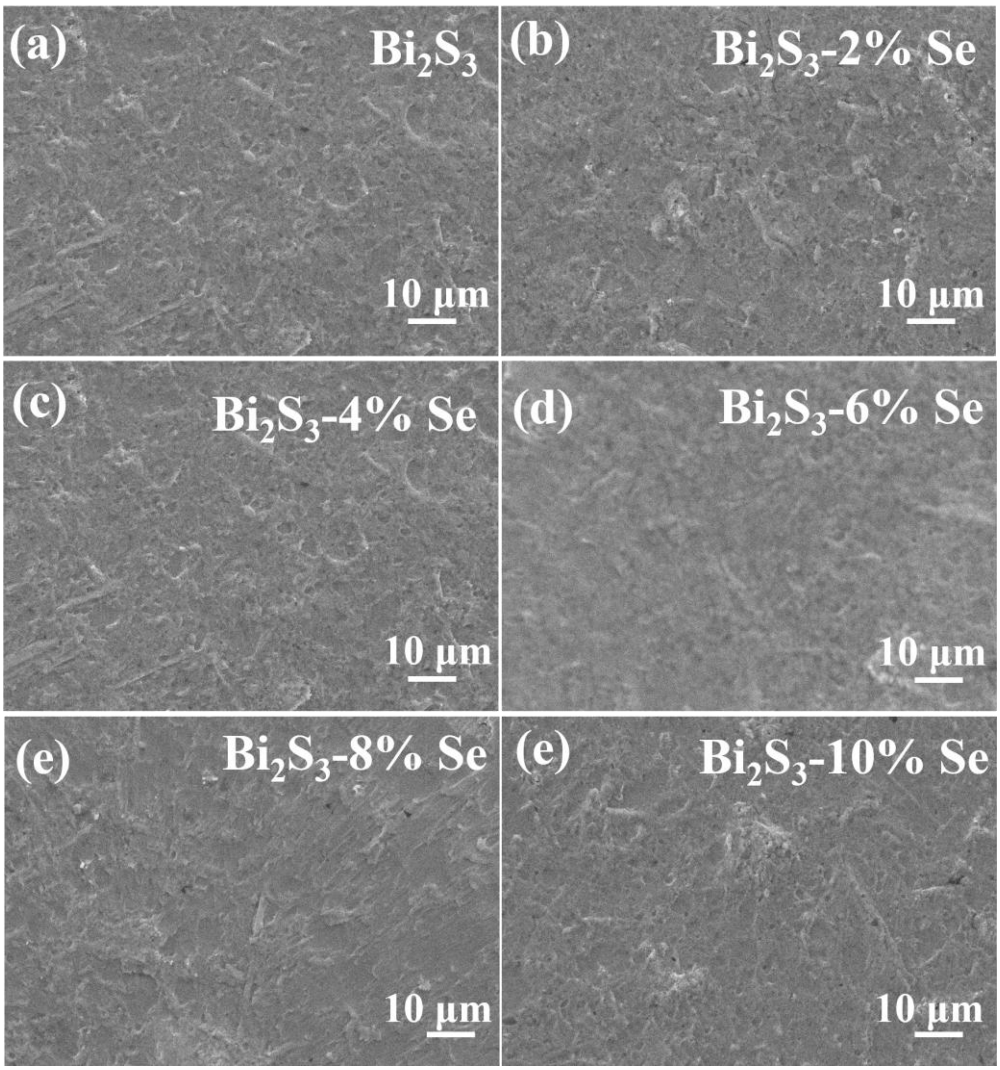

Fig. S8 SEM images of pressed tablets with varying selenium addition amounts.

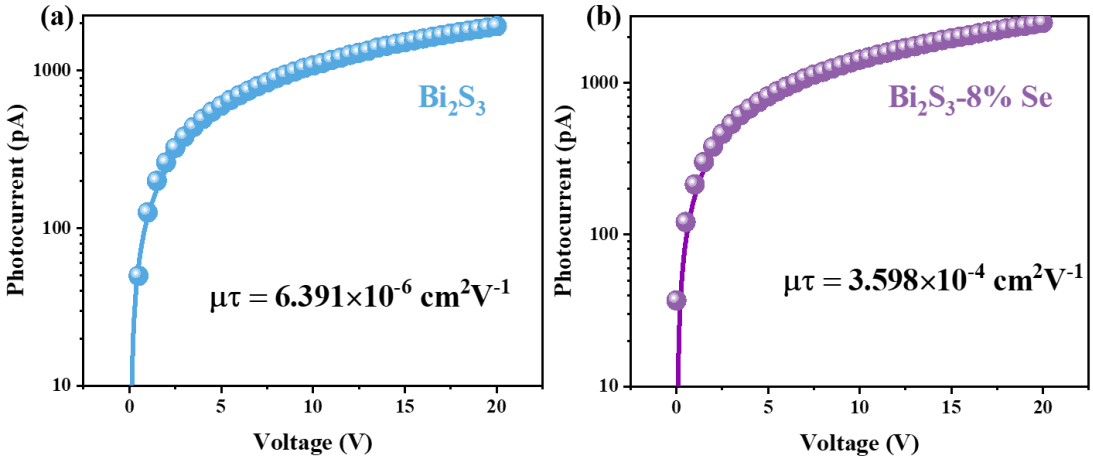

Fig. S9 The Raman spectrum of Bi_2S_3-8% Se, Bi_2S_3 and Bi_2Se_3.

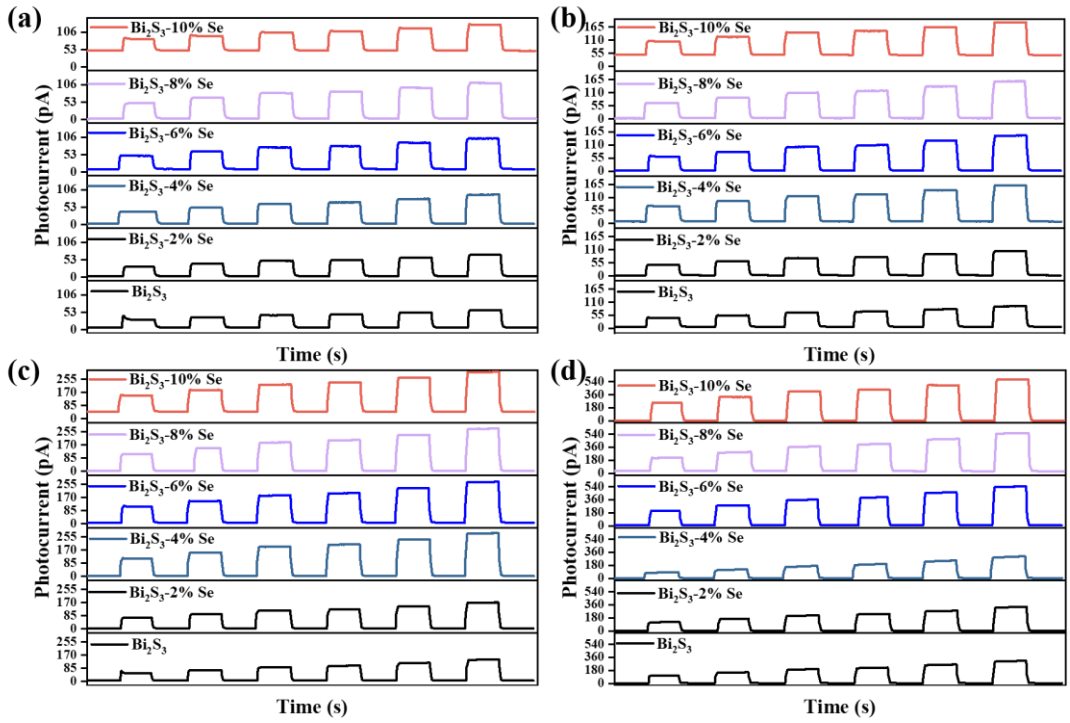

Fig. S10 The photocurrent of different samples under (a) 40 kV, (b) 50 kV, (c) 70 kV, and (d) 120 kV (10 V bias).

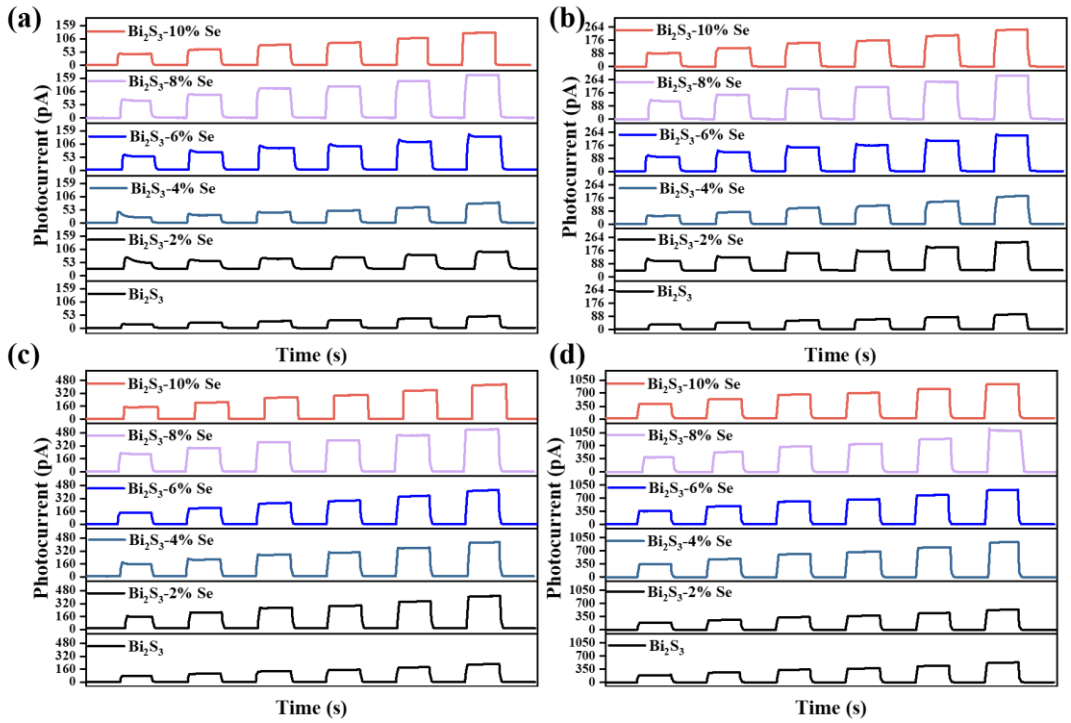

Fig. S11 The photocurrent of different samples under (a) 40 kV, (b) 50 kV, (c) 70 kV, and (d) 120 kV (20 V bias).

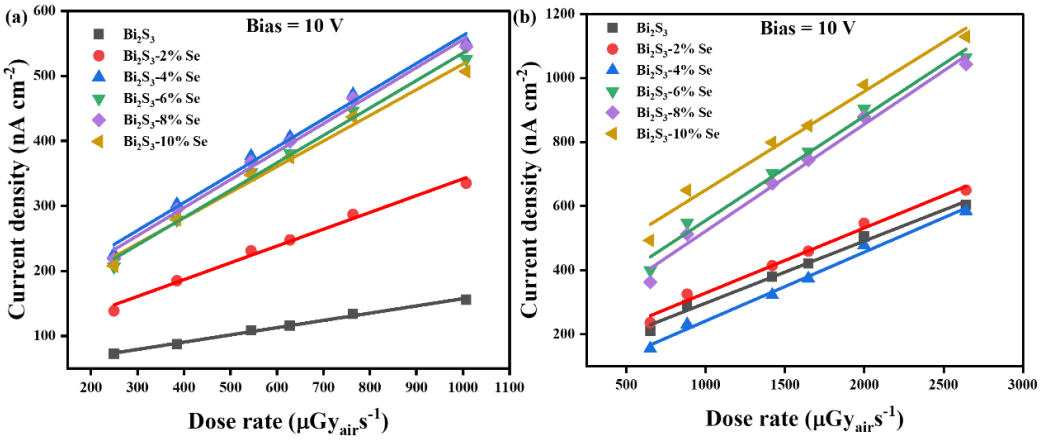

Fig. S12 Photocurrent densities of different samples under (a) 70kV and (b) 120kV. (10 V bias).

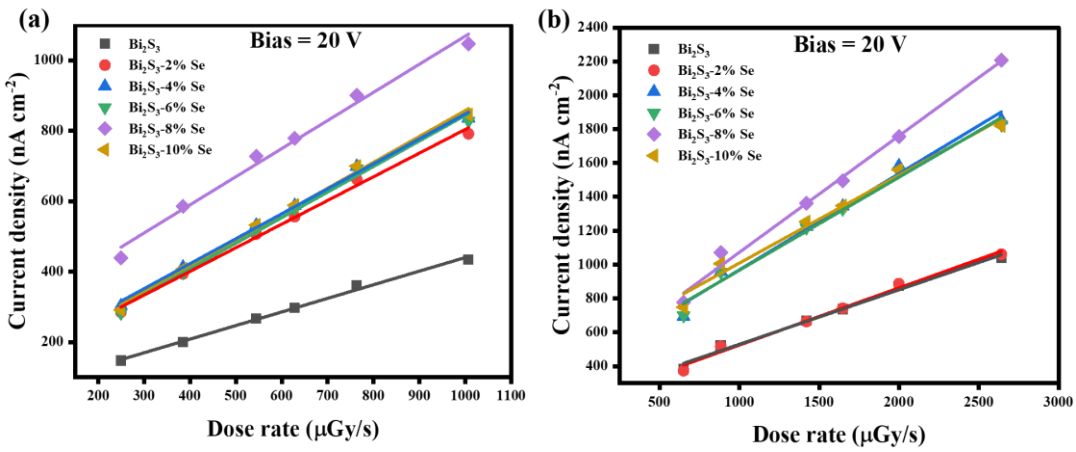

Fig. S13 Photocurrent densities of different samples under (a) 70 kV and (b) 120kV. (20 V bias).

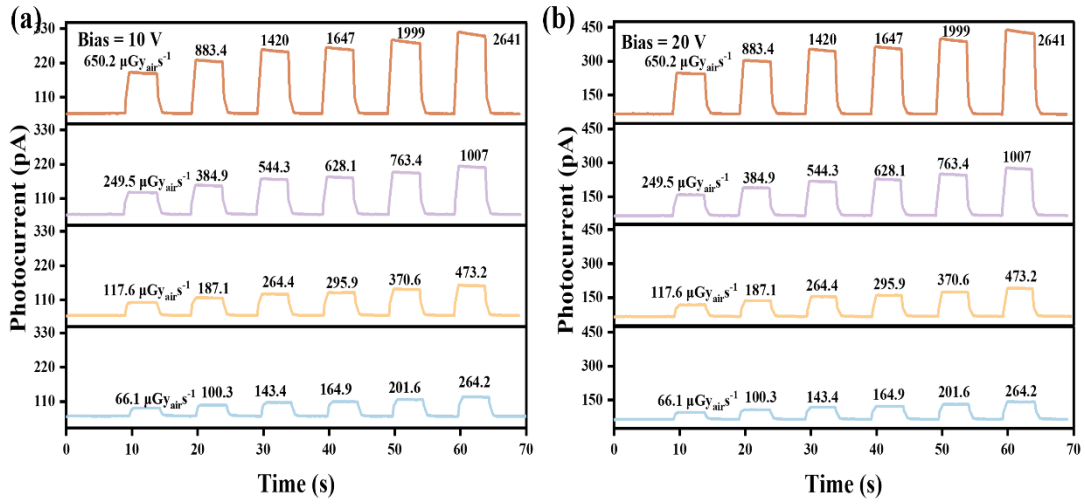

Fig. S14 The photoresponse of the pure Bi_2Se_3 device under 40 kV X-ray irradiation with varing dose rate at (a) 10 V bias and (b) 20 V bias.

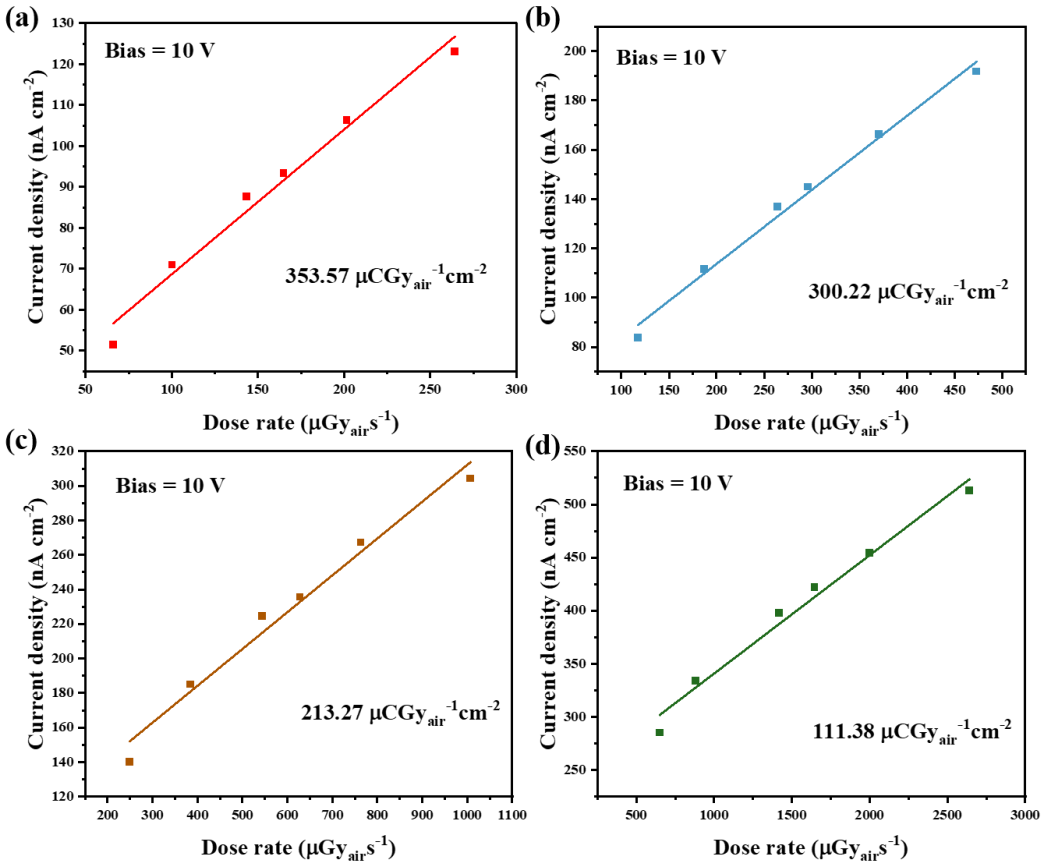

Fig. S15 Current density of the pure Bi_2Se_3 device at 20 V bias under varying X-ray tube voltage. (a) 40 kV, (b) 50 kV, (c) 70 kV and (d) 120 kV.

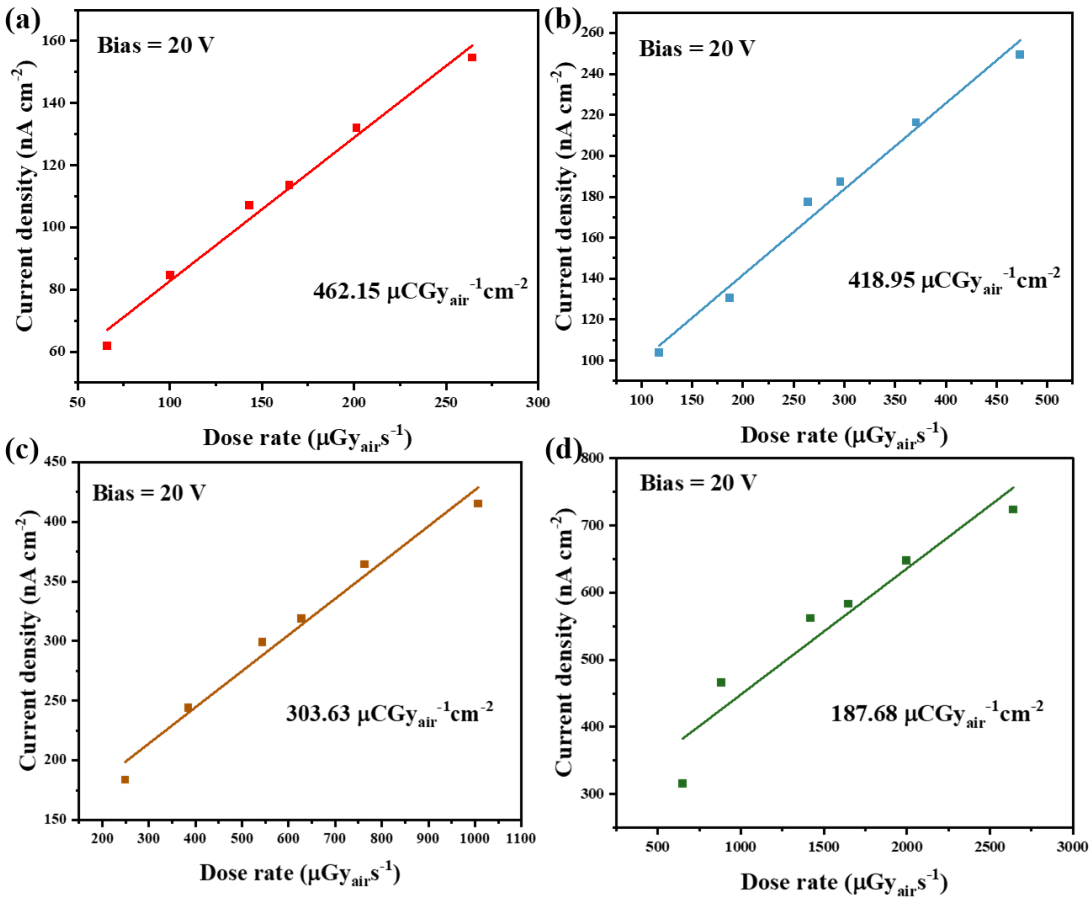

Fig. S16 Current density of the pure Bi_2Se_3 device at 20 V bias under varying X-ray tube voltage. (a) 40 kV, (b) 50 kV, (c) 70 kV and (d) 120 kV.

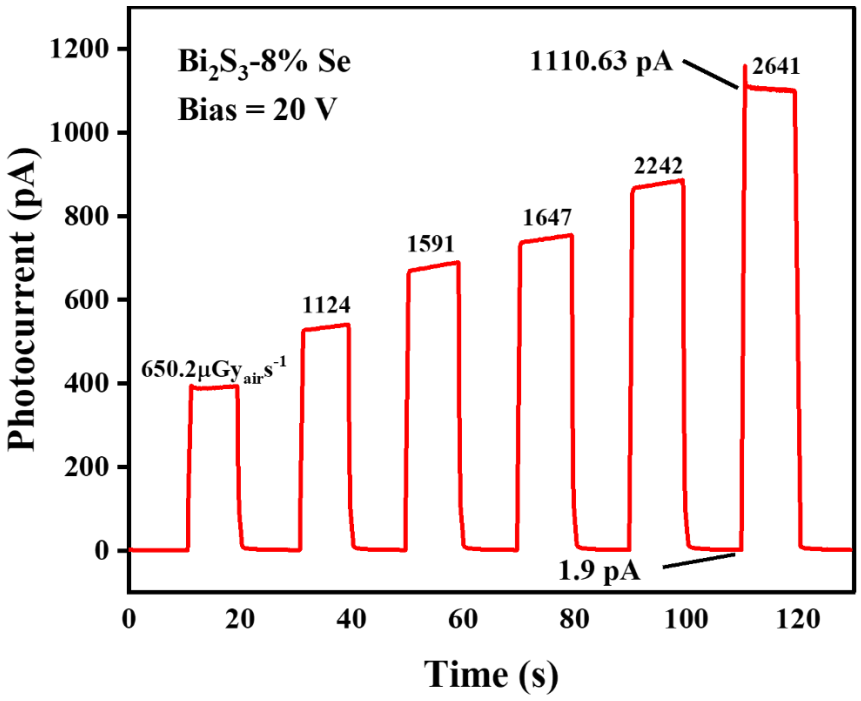

Fig. S17 The photocurrent of Bi_2S_3-8% Se under 20 V and 120 kV tube voltage.

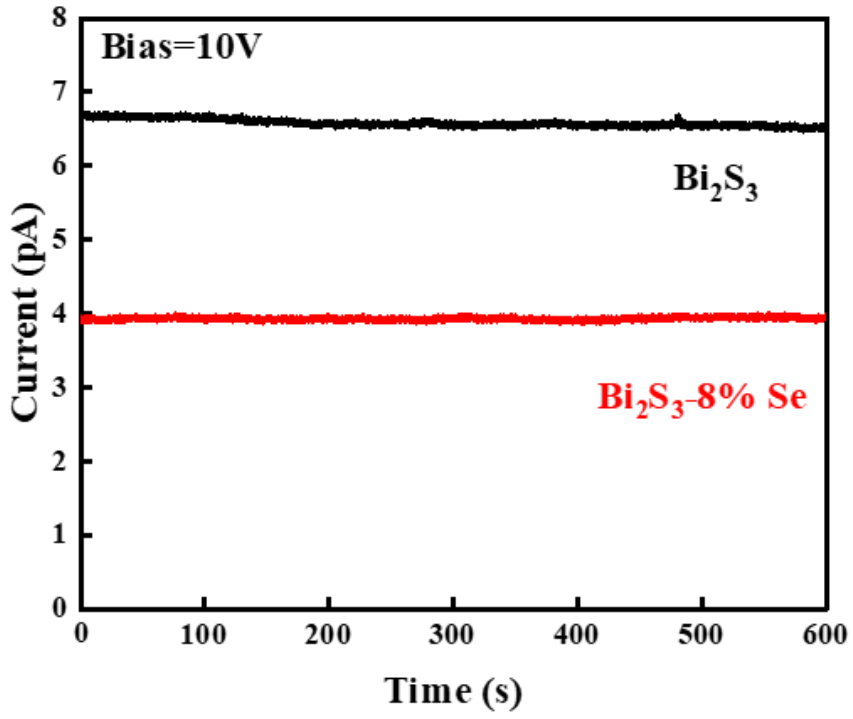

Fig. S18 Stability of the dark current for Bi2S3 and Bi2S3-8% Se-based detectors at 10V.

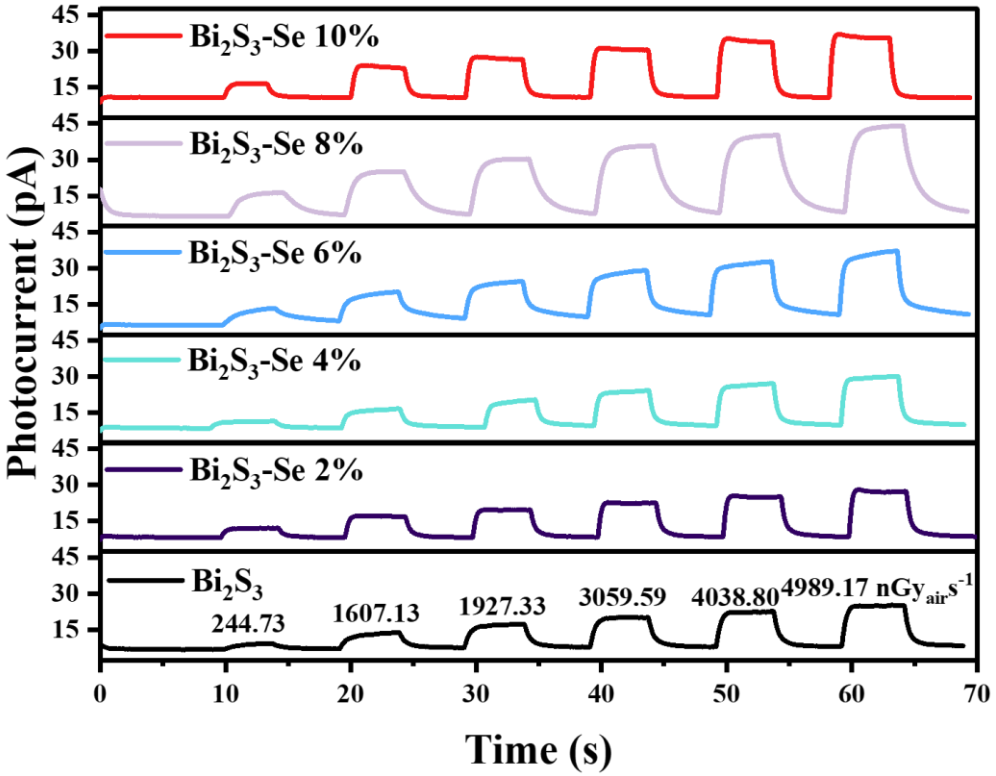

Fig. S19 Photocurrent of different samples under low dose rates.

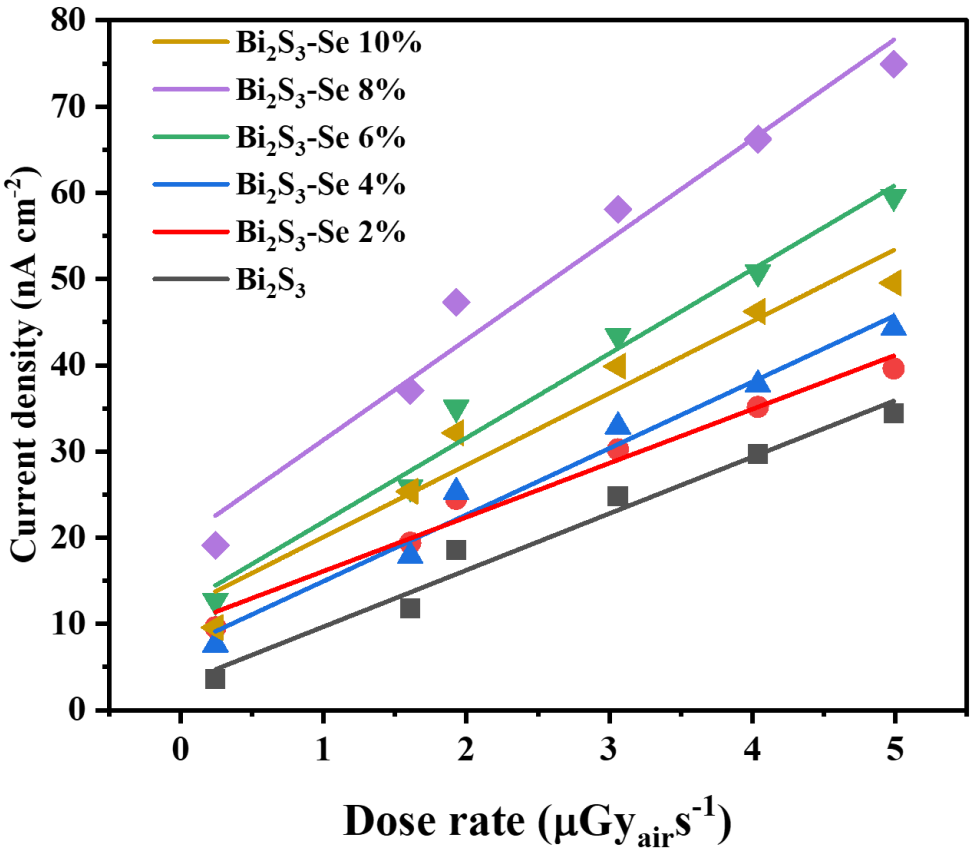

Fig. S20 Photocurrent densities of various samples under low dose rates.

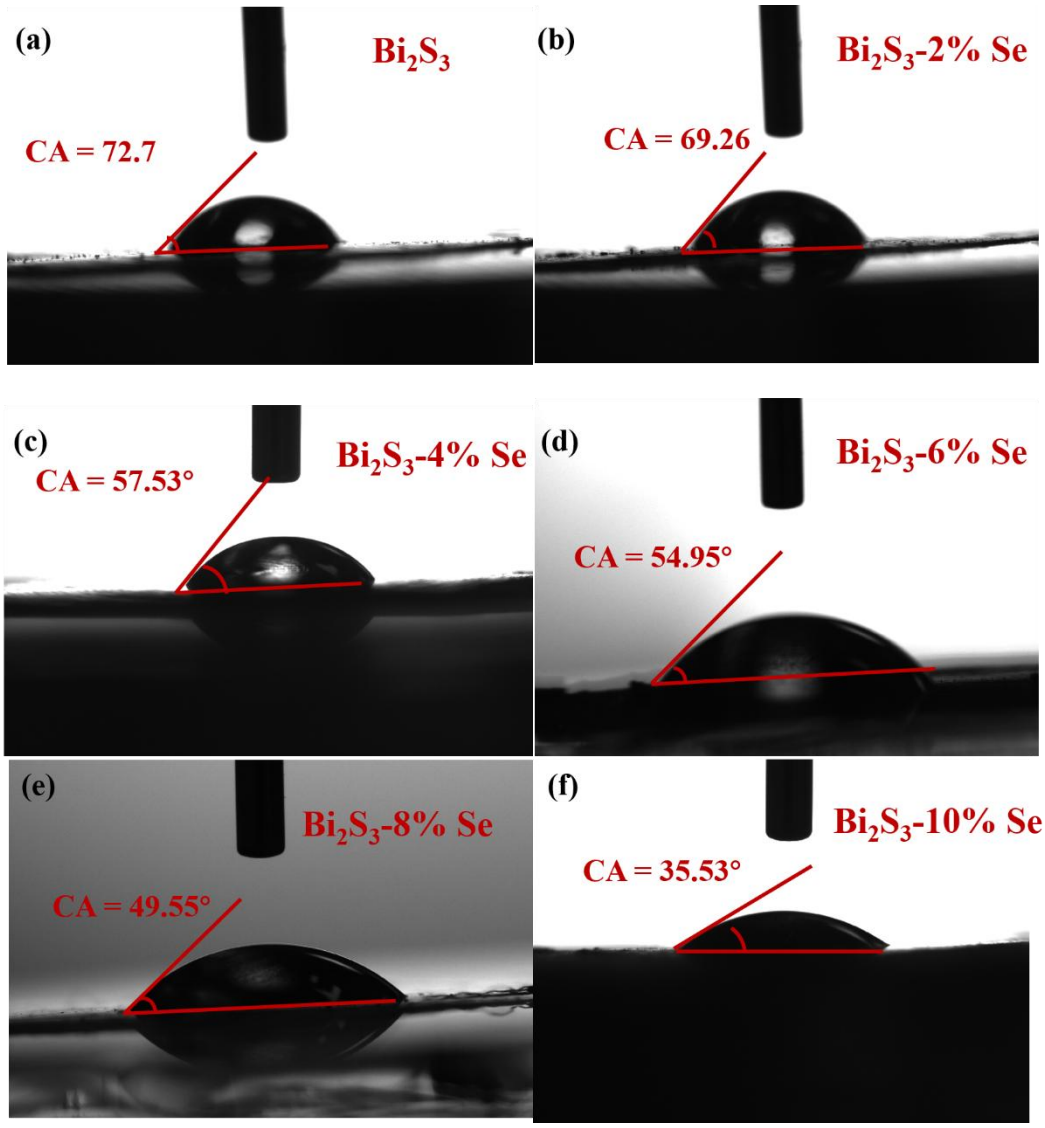

Fig. S21 Surface contact angles of different samples.

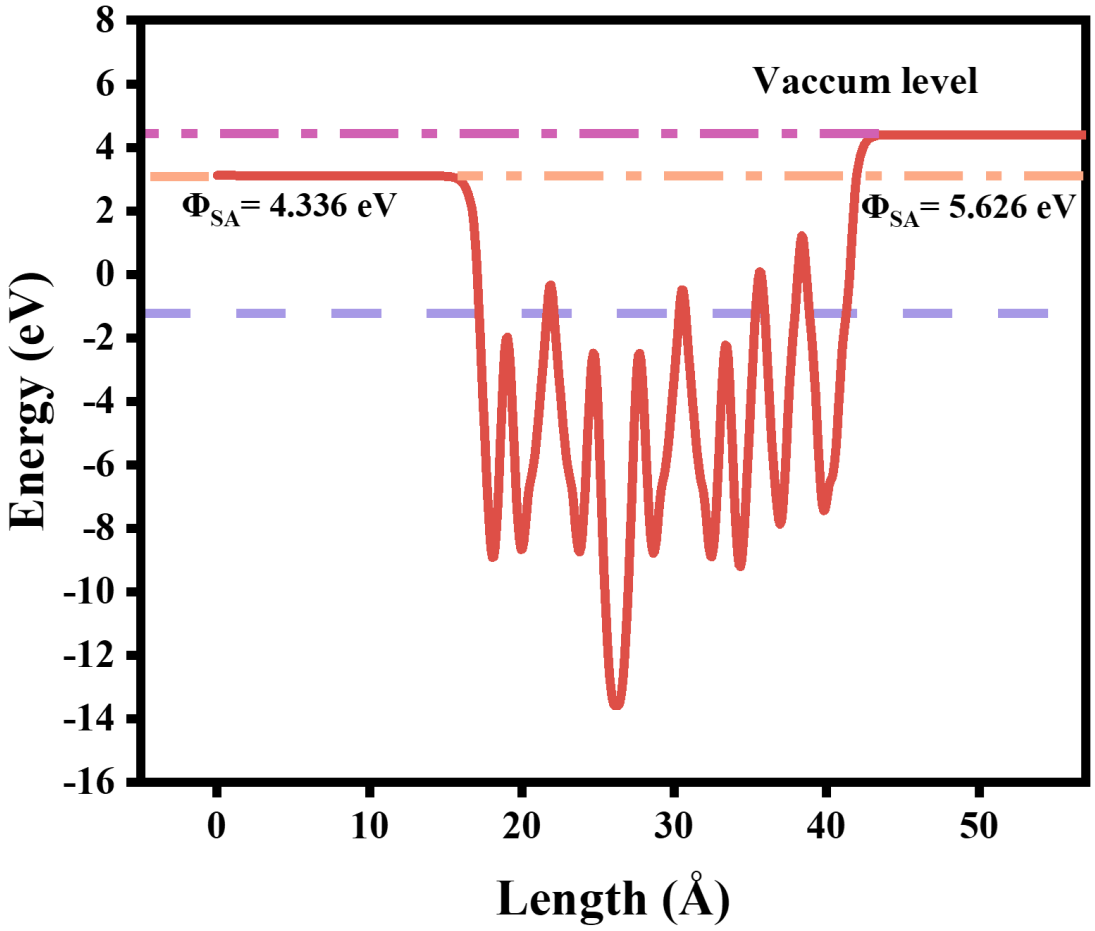

Fig. S22 Calculated work function schematic illustration of fermi level variation.

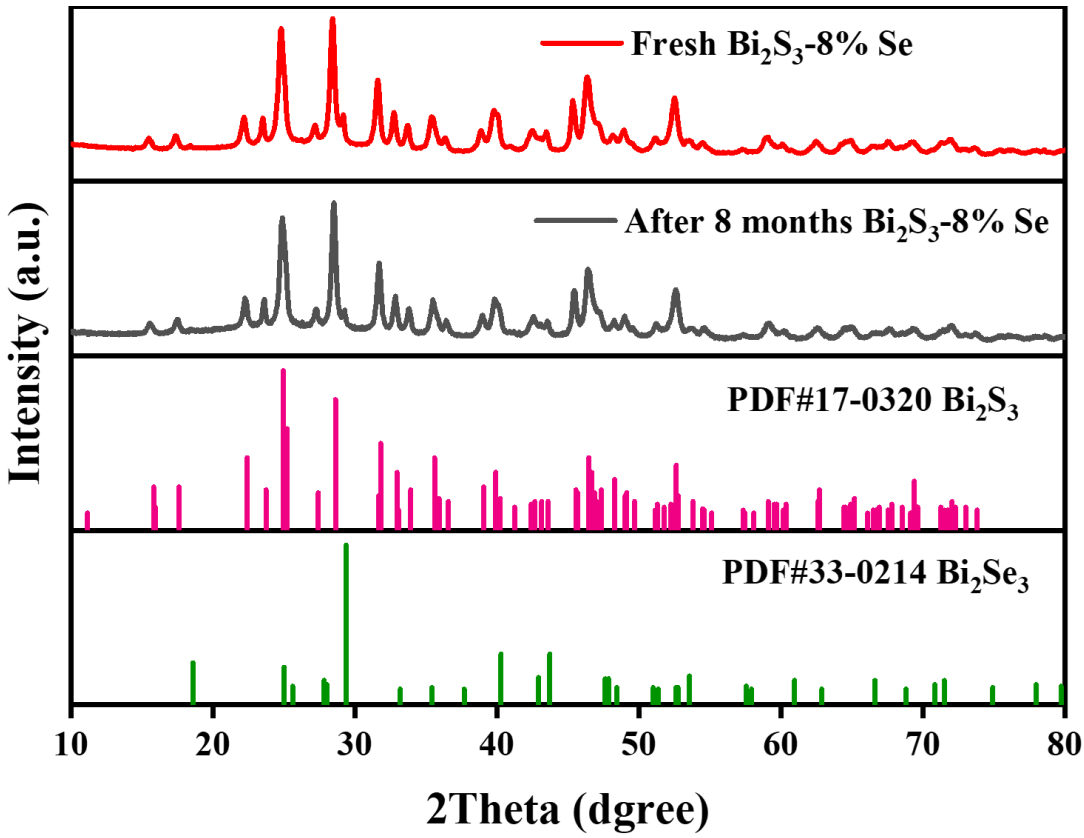

Fig. S23 XRD patterns between fresh Bi_2S_3-8% Se sample and the sample after 8 months of storage under ambient condition.